Corrosion Science 66 (2013) 256–262

Contents lists available at SciVerse ScienceDirect

Corrosion Science

journal homepage: www.elsevier.com/locate/corsci

The effect of sulfide on the aerobic corrosion of carbon steel in near-neutral pH saline solutions

B.W.A. Sherar [a,*], P.G. Keech [b], D.W. Shoesmith [c]

[a] Blade Energy Partners, Ltd., 16285 Park 10 Place, Suite 600, Houston 77084, TX, United States
[b] Nuclear Waste Management Organization, 22 St. Clair Avenue East, Toronto, ON, Canada M4T 2S3
[c] University of Western Ontario, Department of Chemistry, 1151 Richmond Street, London, ON, Canada N6A 5B7

ARTICLE INFO

Article history:
Received 4 August 2012
Accepted 15 September 2012
Available online 1 October 2012

Keywords:
A. Mild steel
B. Polarization
B. SEM
B. Raman spectroscopy
C. Oxygen reduction
C. Microbiological corrosion

ABSTRACT

Severe corrosion damage may occur when gas transmission pipelines are exposed, at disbonded coating locations, to trapped waters containing sulfide followed by secondary exposure to air. Aerobic corrosion with sulfide was investigated in a long-term corrosion experiment in which corrosion was monitored by measurement of the corrosion potential and polarization resistance obtained from linear polarization resistance measurements. The properties and composition of the corrosion product deposits formed were determined using scanning electron microscopy, energy dispersive X-ray analysis, and Raman spectroscopy. A switch from aerobic to aerobic-with-sulfide corrosion doubles the relative corrosion rate.

1. Introduction

Gas transmission pipelines are protected by a combination of coatings and cathodic protection (CP). External corrosion of buried pipeline steel occurs when coatings, used to protect the steel, disbond, exposing the steel to groundwater and inhibiting the effectiveness of CP [1,2]. Based primarily on field inspections of coating failure sites [1,2], TransCanada PipeLines Ltd. (TCPL, Calgary, Alberta, Canada) has proposed six corrosion scenarios that lead to pipeline damage [1,2]. One particularly damaging scenario involves anaerobic corrosion with microbial effects which turn aerobic, and accounts for 17% of all reported coating failures [1,2].

High corrosion rates (2–5 mm yr^{-1} [2]) are associated with this corrosion scenario as iron(II) sulfides oxidize to form iron(III) oxides and elemental sulfur or sulfate [1]. This occurrence means that both Fe and S species are susceptible to oxidation, and the sulfur produced quickly further oxidizes to sulfite or sulfate, which can increase acidity. Difficulties in simulating complex field conditions in the laboratory have meant that only a limited number of experiments have accurately characterized the complex chemical and biological interactions between bacteria and pipeline steel [3,4], and few studies have comprehensively examined the galvanic couple between the pipe and the dispersed sulfide-rich corrosion deposits that help sustain the high corrosion rates observed at field sites [4,5]. Previously, Sherar et al. [6] demonstrated that the iron sulfide formed using both biological and inorganic sulfide sources was mackinawite ($Fe_{1+x}S$), consistent with published literature results [7,8]. As a general field, MIC has been extensively studied and recently reviewed [9–12].

Studies of iron in the presence of inorganic sulfide have been performed, but primarily in acidic [13,14] and alkaline [15,16] solutions not immediately relevant to neutral groundwater conditions. Hansson et al. monitored the influence of adding sulfide to iron specimens pre-exposed to deaerated 0.12 mol L^{-1} $NaHCO_3$ (pH = 9.25 ± 0.15) [17]. Over 10 days of open-circuit exposure, they observed the development of a poorly crystalline FeS identified by Raman spectroscopy as mackinawite. The simultaneous Raman observation of α-FeOOH and polysulfides, however, suggest that conditions were not completely deaerated. While Hansson et al. [17] provide an initial scenario for iron sulfide formation, the duration of their experiments is too short to allow a direct comparison to results obtained in the field.

Recently, Sherar et al. investigated the effect of inorganic sulfide on carbon steel corrosion in a solution containing chloride, bicarbonate and sulfate (pH 8.9) [18] by following the evolution of corrosion potential (E_{CORR}) and periodically measuring the polarization resistance (R_P) over an exposure period of a few months. When freshly-polished carbon steel was exposed directly to sulfide a low corrosion rate (expressed as the reciprocal of the measured polarization resistance [R_P^{-1}; $(5 \pm 1) \times 10^{-5}$ ohm^{-1} cm^{-2}]) was observed; however, when sulfide was added to pre-corroded steel, the corrosion rate tripled [18]. These observations were consistent with the results reported by Newman et al. [19],

* Corresponding author. Tel.: +1 281 961 1283; fax: +1 281 206 2005.
E-mail address: bsherar@blade-energy.com (B.W.A. Sherar).

0010-938X/$ - see front matter © 2012 Elsevier Ltd. All rights reserved.
http://dx.doi.org/10.1016/j.corsci.2012.09.027

who hypothesized that a pre-corroded surface prevents FeS passivation. In their work, polished electrodes exposed to 15 mmol L^{-1} HS^- would passivate ($[R_P^{-1}] < 2 \times 10^{-5}$ ohm^{-1} cm^{-2}) within eight days. However, electrodes pre-corroded in a low sulfide solution (0.6 mmol L^{-1} HS^-) and then later exposed to a higher concentration (15 mmol L^{-1} HS^-) would not passivate ($R_P > 5 \times 10^{-4}$ - ohm^{-1} cm^{-2}) [19].

Previously, we have studied the influence of anaerobic–aerobic cycling on the corrosion of carbon steel in near-neutral pH simulated groundwaters [18,20,21] in the absence of any sulfide, since this is one identified route for the accumulation of significant pipeline damage [1,2]. A sequence of such cycles, over a period of 238 days, lead to corrosion localized within tubercles with most of the corrosion leading to an increased depth of penetration beneath the tubercle cap [18,20,21]. Surrounding the tubercles was a thick magnetite/maghemite film, as a consequence of a sequence of anaerobic–aerobic corrosion cycles [20,21]; the addition of sulfide had no immediate effect on the corrosion rate [18]. The presence of small amounts of mackinawite on the oxide surface implies minor chemical conversion of the thick film, suggesting that corrosion rates could eventually increase [18].

In the present article, we investigate the influence of sulfide and aeration on such a corrosion scenario using our previously developed methodology [18,20,21]. E_{CORR} was monitored and R_P^{-1} values were obtained periodically using linear polarization resistance (LPR) measurements. Subsequently, the morphology and composition of the corrosion product deposits were determined using scanning electron microscopy (SEM) and energy dispersive X-ray spectroscopy (EDX), and Raman spectroscopy.

2. Experimental details

2.1. Materials and electrode preparation

Experiments were performed with X65 carbon steel (0.07 C; 1.36 Mn; 0.013 P; 0.002 S; 0.26 Si; 0.01 Ni; 0.2 Cr; 0.011 Al [wt.%]) with a balance of Fe (procured from TCPL). For corrosion measurements, cubic coupons, 1.0 × 1.0 × 1.0 cm, were cut from metal plates and fitted with a carbon steel welding rod (4 mm diameter), to facilitate connection to external equipment. Electrodes and specimens were then encased in a high performance epoxy resin (Ameron pearl grey resin and 90HS cure) with only a single face exposed to prevent exposure of the electrical contact to the solution. Prior to each experiment, the exposed face (surface area 1.0 cm^2) was ground sequentially on 180, 320, 600, and 1200 grit silicon carbide paper, and then ultrasonically cleaned for ten minutes in deaerated, ultrapure de-ionized water (Millipore, conductivity: 18.2 MΩ cm) mixed with methanol at a ratio of 1:1 to remove organics, and finally ultrasonically cleaned in Millipore water.

2.2. Solution

The experiment was conducted in an aqueous solution containing research grade 0.2 mol L^{-1} $NaHCO_3$ + 0.1 mol L^{-1} NaCl + 0.1 mol L^{-1} Na_2SO_4. This solution was chosen to allow comparison to previous measurements [20–25]. The pH was set to 8.90 ± 0.05 with NaOH or HCl prior to beginning the experiment.

Anaerobic conditions were maintained by placing the cell in an anaerobic chamber ($[O_2] < 1$ ppm), while aerobic conditions were maintained by venting the cell with air after removal from the anaerobic chamber. Following a period of aerobic corrosion, aliquots of HS^- (source: 0.1 mmol L^{-1} $Na_2S{\cdot}9H_2O$ stock solution) were added using a micropipette.

2.3. Electrochemical cell and equipment

The experiment was conducted in a standard three-compartment, three-electrode glass electrochemical cell. The counter electrode was a Pt foil (99.9% purity, Alfa Aesar) and the reference electrode a commercial saturated calomel electrode (SCE; 241 mV vs. SHE) (Radiometer Analytical, Loveland, CO). The cell was either housed in a grounded Faraday cage or placed in a grounded anaerobic chamber; both locations minimize external noise. Prior to immersion of the steel coupons, the electrolyte solution was purged for at least one hour in ultra high purity Ar (Praxair, Mississauga, ON) to generate anaerobic conditions. Each experiment was performed using either a Solartron 1480 Multistat or a Solartron 1287 Potentiostat, running Corrware software (version 2.6 (Scribner Associates)) to control applied potentials and to record current responses.

2.4. Experimental procedure

The ground steel electrode was exposed to anaerobic conditions prior to aerobic corrosion followed by aerobic corrosion with additions of sulfide. Additional specimens were exposed to the same solution and used in subsequent analyses. The electrode and specimens were cathodically cleaned at −1.3 V_{SCE} for one minute to reduce any air-formed surface oxide. The potential was then stepped to −1.1 V_{SCE} for one minute to reduce H_2 production and clear the surface of H_2 bubbles while maintaining cathodic protection. The corrosion potential (E_{CORR}) was then monitored continuously, except for brief periods (every 24 h) during which the polarization resistance (R_P) was measured using the linear polarization resistance (LPR) technique. LPR measurements were performed by scanning the potential ±10 mV from E_{CORR} at a scan rate of 0.1 mV s^{-1}, and a single measurement required a total of 10 min. The current values observed during LPR measurements ranged from 5 to 50 μA cm^{-2} under anaerobic conditions, and from 100 to 150 μA cm^{-2} under aerobic conditions. Periodically, specimens were removed for surface analysis and not subsequently replaced in the cell [20].

2.5. Surface analysis

Specimens and electrodes removed from solution during, or on completion of, an experiment were quickly rinsed in deaerated, Millpore water to prevent the precipitation of the electrolyte. Specimens were dried in the anaerobic chamber to minimize exposure to air during transfer for surface analysis. The electrode and specimens were analyzed by scanning electron microscopy (SEM), energy dispersive X-ray (EDX) analysis, and Raman spectroscopy. SEM was performed along with EDX to elucidate the morphology of corrosion deposits and to determine their elemental composition using a Hitachi S4500 field emission SEM and employing a primary beam voltage of 10 kV. To identify iron oxide/sulfide phases, a Renishaw 2000 Raman spectrometer, with a 632.8 nm laser line and an optical microscope with a 50× magnification objective lens, were used. The expected Raman peak positions for various Fe oxide/sulfide phases are summarized in Table 1 [7,26–28].

3. Results and discussion

The steel was subjected to an anaerobic corrosion period of 28 days followed by a 38 day period of aerobic corrosion prior to the introduction of sulfide. While this is not a corrosion scenario specifically identified by TCPL [1,2,4], it was explored to determine the influence of sulfide on an already corrosion-damaged surface.

Table 1
Expected Raman peak positions for various iron phases.

Compound	Composition	Raman Shift (cm^{-1})	Reference
Hematite	α-Fe_2O_3	226, 292, 406, 495, 600, 700	[26]
Goethite	α-FeOOH	297, 392, 484, 564, 674	[26]
Mackinawite	$Fe_{(1+x)}S$	254, 307, 318, 354	[7]
Maghemite	γ-Fe_2O_3	358, 499, 678, 710	[26]
Magnetite	Fe_3O_4	297, 523, 666	[26]
Siderite	$FeCO_3$	734, 1089, 1443, 1736	[27]
Sulfur	S_8	150, 220, 475	[28]

Fig. 1 shows E_{CORR} (line) and R_P^{-1} (data points) as a function of time.

During the initial anaerobic period, E_{CORR} remained below -800 mV_{SCE} for the entire 28 days, and R_P^{-1} remained $<1 \times 10^{-4}$ ohm^{-1} cm^{-2} consistent with the previously observed anaerobic corrosion behavior [2,22,29,30]. On switching from anaerobic to aerobic conditions (day 28), both E_{CORR} and R_P^{-1} increased rapidly to -430 mV_{SCE} and $>8 \times 10^{-4}$ ohm^{-1} cm^{-2}, respectively (Fig. 1). Subsequently, E_{CORR} slowly decreased and, after passing through a shallow minimum value at ~35 days, increased to a final steady-state value of -530 mV_{SCE}. These changes in E_{CORR} were accompanied by a decrease and increase in R_P^{-1}, with a maximum value in R_P^{-1} being achieved at the minimum value in E_{CORR}. This suggests that, despite the decrease in R_P^{-1} between days 28 and 30, the overall consequence of the decrease in E_{CORR} prior to the shallow minimum (35 days) is an increased activation of the steel surface. Beyond this maximum in R_P^{-1} the minor increase in E_{CORR} was accompanied by a slight, but steady, decrease in R_P^{-1}. While this minor decrease in R_P^{-1} does not indicate passivation, it does suggest that the accumulation of an oxidized corrosion product layer led to a minor suppression of the overall corrosion rate. Despite the fact that the LPR method yields an average R_P^{-1} value for the entire surface, it cannot discount or detect ongoing localized corrosion (e.g. pitting) phenomena.

The first addition of sulfide led to an immediate 50 mV decrease in E_{CORR} to -600 mV_{SCE}, accompanied by a substantial increase in R_P^{-1} up to ~1.8×10^{-3} ohm^{-1} cm^{-2}. After ~2 days, E_{CORR} increased again and R_P^{-1} decreased. This behavior implies that local sites, activated on addition of sulfide were, at least partially, passivated by iron sulfide formation. Over the following 3 days E_{CORR} decreased slightly and R_P^{-1} increased, suggesting the gradual conversion of the more inhibiting oxide to a less protective iron sulfide [17,31,32]. Three further additions of sulfide, leading to a final total [HS^-] of 3.75 mmol L^{-1}, generated similar transients in E_{CORR} and R_P^{-1}. At an [HS^-] of 3.75 mmol L^{-1}, R_P^{-1} was 3× the value recorded prior to the first HS^- addition. This implies that the overall influence of HS^- under aerobic conditions was to decrease the protectiveness of surface deposits and/or stimulate steel dissolution at localized pores.

Fig. 2a and b show SEM micrographs of the specimen surface after exposure to the anaerobic solution for 27 days. Polishing lines are still visible, indicating that limited corrosion occurred, as expected based on the very low corrosion rates (proportional to R_P^{-1}) measured over this exposure period. Fig. 2c is an EDX spot analysis of the surface showing the presence of Fe, C, Na, and Si. The presence of Na and Si are not particularly important for this investigation, however their presence on specimen surface is possible. We commonly detect traces of Na, which may come from the electrolyte used, and Si (and sometimes Al), which may come from either steel impurities or grinding residuals. The weak O signal, and present as a shoulder on the Fe peak, at ~0.7 keV, confirms that only a thin oxide is present. (When the oxide is thicker, this O peak is clear and easily resolved from the iron peak [see Fig. 5b) At the E_{CORR} prevailing in this experiment (<-800 mV_{SCE}, Fig. 1) and in the absence of obvious deposited siderite ($FeCO_3$) crystals, it is likely that this thin layer is magnetite (Fe_3O_4), although this was not confirmed by Raman or other analyses.

Fig. 3a is a low magnification SEM micrograph of the electrode after 29 days of anaerobic corrosion followed by 33 days of aerobic corrosion (day 62). The most prominent features are the localized tubercles. Fig. 3b is a close up of the surface surrounding the localized tubercles. The finely particulate corrosion product deposit was not evident prior to aerobic exposure (Fig. 2). Fig. 4a shows a Raman spectrum recorded on a visibly orange tubercle, and indicates the presence of goethite, α-FeOOH (peaks at 245, 299, 397, 471, 553, and 678 cm^{-1} compared to reference peak positions of 297, 392, 484, 564, and 674 cm^{-1} [26]) and magnetite (299 and

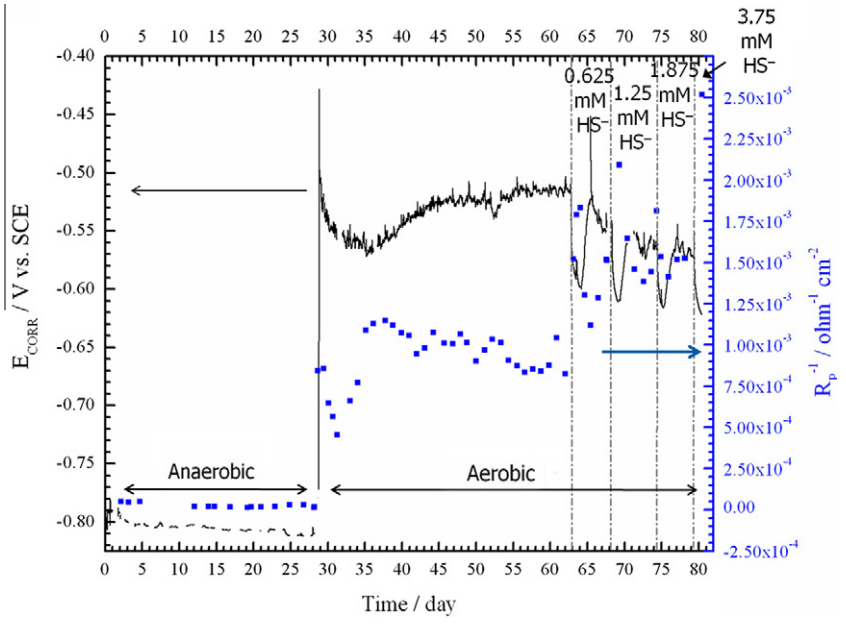

Fig. 1. The change of corrosion potential (E_{CORR}; line) and inverse polarization resistances (R_P^{-1}; data points) of steel measured under anaerobic followed by aerobic conditions. Aliquots of HS^- were added during various stages during this aerobic period. The labeled HS^- concentration is cumulative for a specific period.

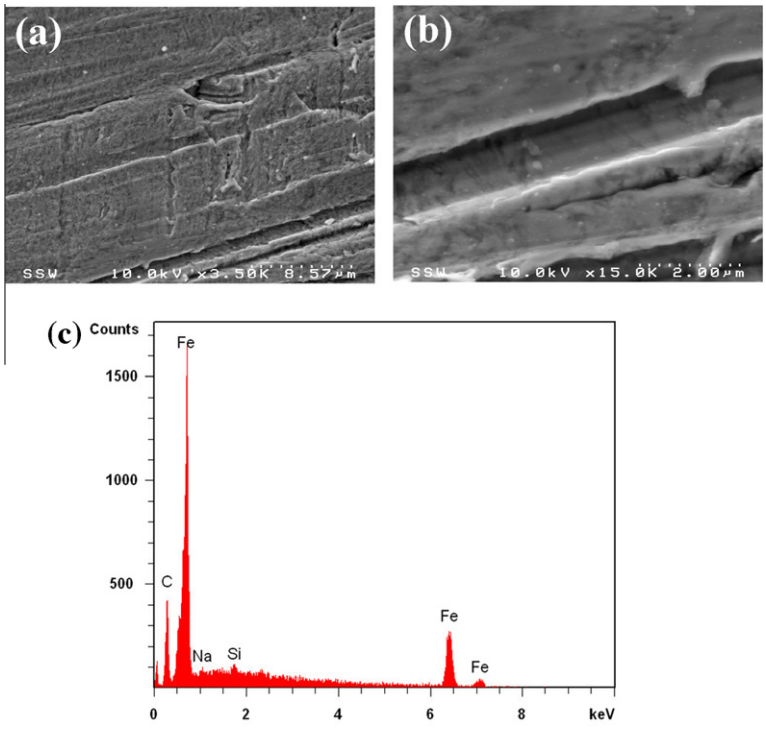

Fig. 2. SEM micrographs of steel after anaerobic exposure for 29 days: (a) low magnification image and (b) high magnification image. (c) EDX spot analysis of the surface.

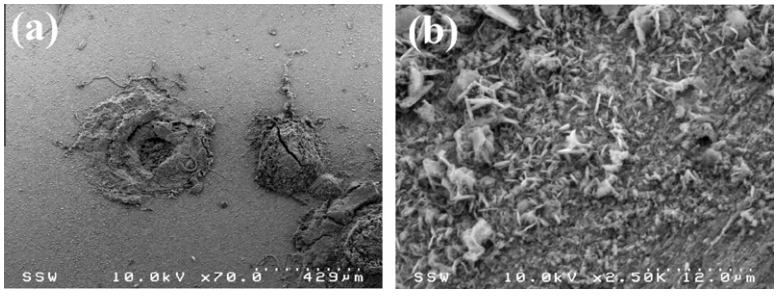

Fig. 3. (a) Low magnification SEM micrograph of tubercles formed on a steel surface after anaerobic (29 days) followed by aerobic (33 days) exposure. (b) High magnification SEM micrograph of surface deposits at locations adjacent to the tubercles shown in (a).

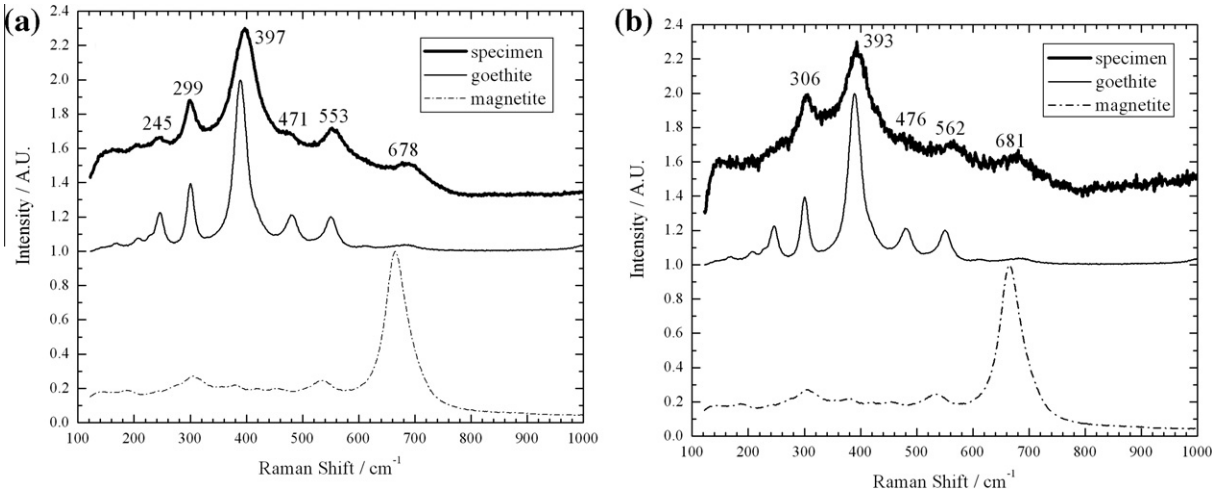

Fig. 4. Raman spectra recorded on (a) a tubercle and (b) the oxide surface adjacent to the tubercles shown in Fig. 3. Standard spectra are shown for comparison.

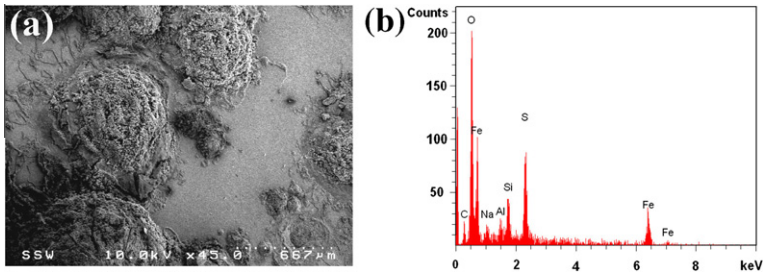

Fig. 5. (a) SEM micrograph of tubercles after anaerobic (29 days), aerobic (33 days), and aerobic corrosion with sulfide (20 days). (b) EDX spectrum of a tubercle shown in (a).

678 cm^{-1}) as the dominant phases. The Raman spectra in Fig. 4b show that the surface adjacent to the tubercles has a similar composition The dominance of goethite is unsurprising in the presence of dissolved O_2 [33]. The very weak Raman peaks at 678 cm^{-1} in a tubercle region (Fig. 4a) and 681 cm^{-1} on the surrounding surface (Fig. 4b) suggest the presence of magnetite, possibly as a layer underneath the goethite.

The appearance of tubercles indicates that the introduction of O_2 induced the separation of anodes and cathodes. Once initiated, corrosion would be expected to concentrate at these locations, with the surrounding surface remaining considerably less reactive as previously demonstrated [17,18]. The scattered nature of the corrosion product deposit on the surface surrounding the tubercles suggests that, after this relatively short exposure period, the goethite surface layer may not be completely protective allowing O_2 reduction in support of active corrosion within the tubercles. A detailed discussion of the reactions leading to the growth of tubercles, including the location of the cathode, has been reported [21].

The surface of the electrode after the full 82 day exposure was completely black on initial removal from the solution, but the tubercles turned partially orange (revealing the goethite layer underneath) consistent with the air oxidation of available Fe(II) species. This conversion from black to orange tubercles was minimized by quickly placing the electrode in an anaerobic chamber to dry. Fig. 5a is a SEM micrograph showing an area of the surface partially occupied by tubercles and associated filiforms. The presence of more and larger tubercles in Fig. 5a compared to Fig. 3a, probably reflects the fact two different surfaces are being analyzed. However, the possibility that a combination of oxygen and sulfide may have caused the initiation of additional tubercles (i.e., more than expected when only oxygen was present) cannot be ruled out. Although individual tubercles are smaller in cross section by width and height, the corrosion morphology is consistent with that observed after successive periods of anaerobic–aerobic cycling, with the last cycle being anaerobic corrosion with sulfide [20]. A cross-sectional area of the pit beneath the tubercle revealed an orange deposit [20]. EDX spot analysis indicates the presence of S on tubercle surfaces, along with Fe, C, and O (Fig. 5b). The O signal was still dominant indicating oxide to sulfide conversion is slow on the time scale of this experiment. The small amounts of Si and Al could result from steel impurities, or from polishing residue. A Raman spectrum recorded on a tubercle, Fig. 6, indicates that goethite remains the dominant phase with magnetite (and possibly mackinawite) also present. A shoulder in the spectrum, around 465 cm^{-1}, could suggest the presence of elemental sulfur (Ref. 475 cm^{-1} [7]). An attempt to curve fit the Raman spectra of the tubercle (post-sulfide exposure) to standard spectra was not performed.

Fig. 7a and b show low and high magnification SEM micrographs of regions of the steel surface not covered by tubercles. A random array of overlapping hexagonal shaped wafers with a density greater than observed in similar locations prior to sulfide addition, Fig. 7b, is observed, indicating HS^- addition lead to enhanced corrosion in these areas. While EDX spot analysis of the general deposit, Fig. 7c, showed S to be present, the relative strength of the O and S peaks indicates the surface remains predominantly oxide-covered. However, Raman analysis (Fig. 8) clearly identifies the presence of mackinawite (254, 302, and 362 cm^{-1}) and probably elemental sulfur (469 cm^{-1}).

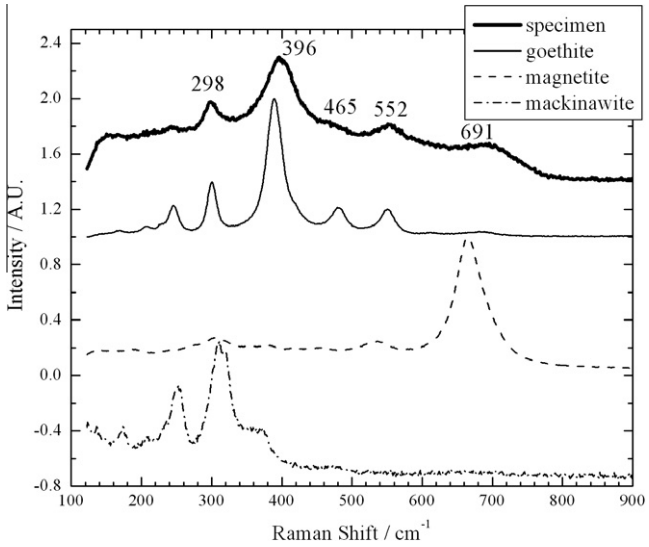

Fig. 6. Raman spectrum recorded on a tubercle (Fig. 5a) compared to standard spectra.

As discussed above, after each successive HS^- addition, E_{CORR} exhibited a transient decrease and recovery, accompanied by a surge and subsequent decrease in R_P^{-1}. The transients, which continued for durations of up to 2 days, suggests the response to HS^- of active locations on the steel surface, and are most likely to be at the exposed steel surface within the tubercles. Given the porosity of the tubercle caps, HS^- penetration at these locations would be expected to lead to a surge in active corrosion (E_{CORR} decrease; R_P^{-1} increase). Since diffusive escape of soluble Fe^{2+} from within the tubercles will be difficult in the presence of the goethite caps, iron sulfide formation, leading to at least partial corrosion inhibition within the tubercle, would also be expected. Under aerobic conditions it is possible that such a reaction could be supported by O_2 reduction on adjacent magnetite surfaces around the edge of the tubercle. Formation of mackinawite within the tubercle underneath the predominantly goethite cap would then explain the failure to unequivocally detect this phase in the Raman analyses of tubercle locations.

A second feature of the corrosion process after HS^- addition is the superposition on the transients described above of an overall

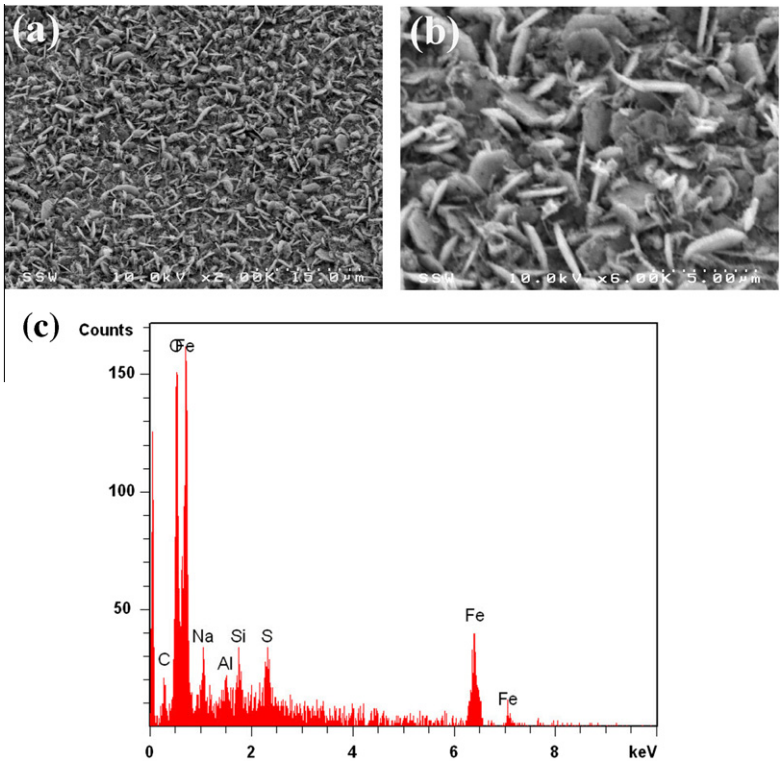

Fig. 7. (a) Low and (b) high magnification images of the steel surface surrounding the tubercles shown in Fig. 5a. (c) EDX spectrum of the same region.

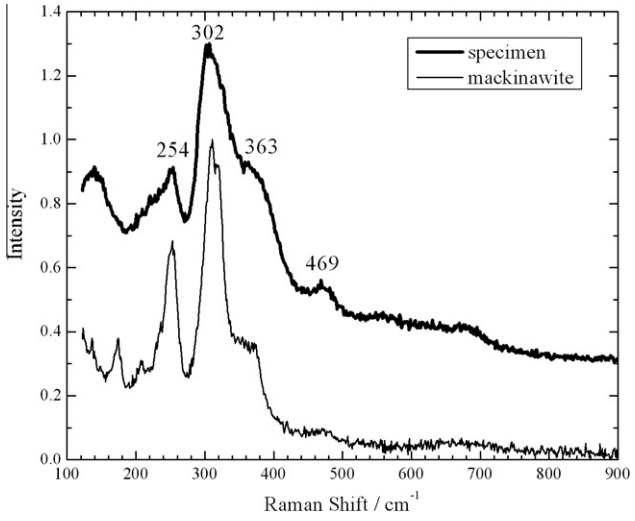

Fig. 8. Raman spectrum recorded on the steel surface surrounding the tubercles shown in Fig. 7a and b. A standard spectrum for mackinawite is shown for comparison.

decrease in E_{CORR} and increase in R_P^{-1} (Fig. 1). This may reflect the steady, more general corrosion process on locations outside the tubercles where mackinawite and sulfur formation are detected. Beyond the time frame of this experiment this overall conversion and activation would be expected to continue and lead to the considerably higher rates and unprotective deposits observed under field conditions. This conversion process is likely to be driven by the reaction of iron(III) oxide with HS^-,

$$Fe_2O_3 + 3HS^- + 3H^+ \rightarrow 2FeS + S + 3H_2O \quad (1)$$

according to the mechanism described by Poulton et al. [32].

Table 2
Summary of calculated averaged inverse polarization resistance (R_P^{-1}) values under specific exposure conditions.

Exposure conditions	Period over which R_P^{-1} was calculated	Averaged R_P^{-1} ($ohm^{-1}\,cm^{-2}$)
(i) Anaerobic	0–28 d	$(3 \pm 1) \times 10^{-5}$
(ii) Aerobic	28–64 d	$(92 \pm 17) \times 10^{-5}$
(iii) Aerobic with HS^-	64–81 d	$(182 \pm 32) \times 10^{-5}$

A comparison of the average R_P^{-1} values measured in the three stages of the experiment is shown in Table 2. A comparison of the R_P^{-1} shows the increase in aggressiveness of the exposure environment is clear in going from anaerobic to aerobic conditions and eventually aerobic conditions in the presence of sulfide. Since these are average R_P^{-1} values (proportional to the corrosion rate only if the process is general) they do not capture the higher absolute values which prevail within local tubercle sites. Also, since the corrosion process is evolving with time from a general to a more localized process, no attempt is made to determine a valid corrosion rate which could be used in a predictive model.

While this experiment was too short to determine what rates are achievable after long term exposure of corroded steel to aerobic sulfide solutions it demonstrates that sulfide would promote destabilization of the oxides on the steel surface especially at locations were localized corrosion conditions prevail; i.e., at tubercle sites. The chemical conversion of the oxide-passivated areas of the surface, while slow, would be expected to persist, and even accelerate, as S is produced by the oxide-sulfide conversion (reaction 1 [31,32,34]), and further oxidized to thiosulfate [35,36] and eventually sulfate [36].

4. Conclusions

(1) A switch from anaerobic to aerobic corrosion lead to an overall increase in E_{CORR} and R_P^{-1}. Aerobic exposure induces the formation of goethite-covered tubercles and a predominately goethite-covered general surface layer. This is consistent with previously reported aerobic corrosion behavior.
(2) The addition of sulfide to the aerobically-exposed surface initiates rapid E_{CORR} and R_P^{-1} transients. Continual sulfide exposure leads to the slow corrosion of the general surface leading to the accumulation of mackinawite. The inability to explicitly detect mackinawite at tubercle sites may indicate sulfide corrosion is confined to regions under the goethite-covered tubercle cap.

Acknowledgements

This research was carried out for NOVA Research & Technology Centre (NRTC, Calgary, AB, Canada) and TCPL through an Industrial Postgraduate Scholarship Agreement with the University of Western Ontario and the Canadian Natural Sciences and Engineering Research Council (NSERC, Ottawa, ON). Fraser King, Integrity Corrosion Consulting Ltd., is gratefully acknowledged by the authors for his guidance and continued support of the research.

References

[1] T.R. Jack, M.J. Wilmott, R.L. Sutherby, Indicator minerals formed during external corrosion of line pipe, Mater. Performance 34 (1995) 19–22.
[2] T.R. Jack, M.J. Wilmott, R.L. Sutherby, R.G. Worthingham, External corrosion of line pipe – a summary of research activities, Mater. Performance 35 (1996) 18–24.
[3] K.H. Williams, S.S. Hubbard, J.F. Banfield, Galvanic interpretation of self-potential signals associated with microbial sulfate-reduction, J. Geophys. Res.-Biogeosci. 112 (2007).
[4] T.R. Jack, A. Wilmott, J. Stockdale, G. Van Boven, R.G. Worthingham, R.L. Sutherby, Corrosion consequences of secondary oxidation of microbial corrosion, Corrosion 54 (1998) 246–252.
[5] R.G. Worthingham, T.R. Jack, V. Ward, External Corrosion of Line Pipe – Part I: Indentification of Bacterial Corrosion in the Field, in: S.C. Dexter (Ed.), In Biologically Induced Corrosion, NACE, Houston, TX, 1986, p. 339.
[6] B.W.A. Sherar, I.M. Power, P.G. Keech, S. Mitlin, G. Southam, D.W. Shoesmith, Characterizing the effect of carbon steel exposure in sulfide containing solutions to microbially induced corrosion, Corros. Sci. 53 (2011) 955–960.
[7] J.A. Bourdoiseau, M. Jeannin, R. Sabot, C. Remazeilles, P. Refait, Characterisation of mackinawite by Raman spectroscopy: effects of crystallisation, drying and oxidation, Corros. Sci. 50 (2008) 3247–3255.
[8] M. Langumier, R. Sabot, R. Obame-Ndong, M. Jeannin, S. Sablé, Ph. Refait, Formation of Fe(III)-containing mackinawite from hydroxysulphate green rust by sulphate reducing bacteria, Corros. Sci. 51 (2009) 2694–2702.
[9] B.J. Little, J.S. Lee, R.I. Ray, Diagnosing microbiologically influenced corrosion: a state-of-the-art review, Corrosion 62 (2006) 1006–1017.
[10] R. Javaherdashti, A brief review of general patterns of MIC of carbon steel and biodegradation of concrete, IUFS J. Biol. 68 (2009) 65–73.
[11] Z. Lewandowski, H. Beyenal, Mechanisms of Microbially Influenced Corrosion, in: H.-C. Flemming, P.S. Murthy, R. Venkatesan, K.E. Cooksey (Eds.), Marine and Industrial Biofouling, Springer, Berlin, DE, 2009, pp. 35–65.
[12] W. Sand, T. Gehrke, Microbially influenced corrosion of steel in aqueous environments, Rev. Environ. Sci. Biotechnol. 2 (2004) 169–176.
[13] H. Ma, X. Cheng, G. Li, S. Chen, Z. Quan, S. Zhao, L. Niu, The influence of hydrogen sulfide on corrosion of iron under different conditions, Corros. Sci. 42 (2000) 1669–1683.
[14] D.W. Shoesmith, P. Taylor, M.G. Bailey, D.G. Owen, The formation of ferrous monosulfide polymorphs during the corrosion of iron by aqueous hydrogen-sulfide at 21-degrees-C, J. Electrochem. Soc. 127 (1980) 1007–1015.
[15] D.W. Shoesmith, M.G. Bailey, B. Ikeda, Electrochemical formation of mackinawite in alkaline sulfide solutions, Electrochim. Acta 23 (1978) 1329–1339.
[16] D.W. Shoesmith, P. Taylor, M.G. Bailey, B. Ikeda, Electrochemical behavior of iron in alkaline sulfide solutions, Electrochim. Acta 23 (1978) 903–916.
[17] E.B. Hansson, M.S. Odziemkowski, R.W. Gillham, Formation of poorly crystalline iron monosulfides: Surface redox reactions on high purity iron, spectroelectrochemical studies, Corros. Sci. 48 (2006) 3767–3783.
[18] B.W.A. Sherar, P.G. Keech, J.J. Noel, D.W. Shoesmith, The effect of sulphide on carbon steel corrosion behaviour in anaerobic near-neutral saline solutions, Corrosion, in press. doi: http://dx.doi.org/10.5006/0687.
[19] R.C. Newman, K. Rumash, B.J. Webster, The effect of precorrosion on the corrosion rate of steel in neutral solutions containing sulfide – relevance to microbially influenced corrosion, Corros. Sci. 33 (1992) 1877–1884.
[20] B.W.A. Sherar, P.G. Keech, D.W. Shoesmith, Carbon steel corrosion under anaerobic–aerobic cycling in near-neutral pH saline solutions – Part 1: Long term corrosion behaviour, Corros. Sci. 53 (2011) 3636–3642.
[21] B.W.A. Sherar, P.G. Keech, D.W. Shoesmith, Carbon steel corrosion under anaerobic-aerobic cycling in near-neutral pH saline solutions – Part 2: Corrosion mechanism, Corros. Sci. 53 (2011) 3643–3650.
[22] B.W.A. Sherar, P.G. Keech, Z. Qin, F. King, D.W. Shoesmith, Nominally anaerobic corrosion of carbon steel in near-neutral pH saline environments, Corrosion 66 (2010) 045001.
[23] Z. Qin, B. Demko, J.J. Noel, D.W. Shoesmith, F. King, R.G. Worthingham, K. Keith, Localized dissolution of millscale-covered pipeline steel surfaces, Corrosion 60 (2004) 906–914.
[24] C.T. Lee, Z. Qin, M. Odziemkowski, D.W. Shoesmith, The influence of groundwater anions on the impedance behaviour of carbon steel corroding under anoxic conditions, Electrochim. Acta 51 (2006) 1558–1568.
[25] C.T. Lee, M.S. Odziemkowski, D.W. Shoesmith, An in situ Raman-electrochemical investigation of carbon steel corrosion in Na_2CO_3/$NaHCO_3$, Na_2SO_4, and NaCl solutions, J. Electrochem. Soc. 153 (2006) B33–B41.
[26] M.A. Legodi, D. de Waal, The preparation of magnetite, goethite, hematite and maghemite of pigment quality from mill scale iron waste, Dyes Pigm. 74 (2007) 161–168.
[27] R.G. Herman, C.E. Bogdan, A.J. Sommer, D.R. Simpson, Discrimination among carbonate minerals by Raman-spectroscopy using the laser microsprobe, Appl. Spectrosc. 41 (1987) 437–440.
[28] S.N. White, Laser Raman spectroscopy as a technique for identification of seafloor hydrothermal and cold seep minerals, Chem. Geol. 259 (2009) 240–252.
[29] N.R. Smart, D.J. Blackwood, L. Werme, Anaerobic corrosion of carbon steel and cast iron in artificial groundwaters: Part 1 – Electrochemical aspects, Corrosion 58 (2002) 547–559.
[30] N.R. Smart, D.J. Blackwood, L. Werme, Anaerobic corrosion of carbon steel and cast iron in artificial groundwaters: Part 2 – Gas generation, Corrosion 58 (2002) 627–637.
[31] S.W. Poulton, Sulfide oxidation and iron dissolution kinetics during the reaction of dissolved sulfide with ferrihydrite, Chem. Geol. 202 (2003) 79–94.
[32] S.W. Poulton, M.D. Krom, R. Raiswell, A revised scheme for the reactivity of iron (oxyhydr)oxide minerals towards dissolved sulfide, Geochim. Cosmochim. Acta 68 (2004) 3703–3715.
[33] J. Detourna, M. Ghodsi, R. Derie, Kinetic study of goethite formation by aearation of ferrous hydroxide gels, Industrie Chimique Belge-Belgische Chemische Industrie 38 (1974) 695–701.
[34] M.D. Afonso, W. Stumm, Reductive dissolution of Iron(III) (hydro)oxides by hydrogen-sulfide, Langmuir 8 (1992) 1671–1675.
[35] C.F. Petre, F. Larachi, Reaction between hydrosulfide and iron/cerium (hydr)oxide: hydrosulfide oxidation and iron dissolution kinetics, Top. Catal. 37 (2006) 97–106.
[36] C.F. Petre, F. Larachi, Capillary electrophoretic separation of inorganic sulfur–sulfide, polysulfides, and sulfur–oxygen species, J. Sep. Sci. 29 (2006) 144–152.